

# The production and persistence of $\Sigma\text{RONO}_2$ in the Mexico City plume

A. E. Perring<sup>1,\*,\*\*</sup>, T. H. Bertram<sup>1,\*\*\*</sup>, D. K. Farmer<sup>1,\*\*</sup>, P. J. Wooldridge<sup>1</sup>, J. Dibb<sup>2</sup>, N. J. Blake<sup>3</sup>, D. R. Blake<sup>3</sup>, H. B. Singh<sup>4</sup>, H. Fuelberg<sup>5</sup>, G. Diskin<sup>6</sup>, G. Sachse<sup>6</sup>, and R. C. Cohen<sup>1,7</sup>

<sup>1</sup>Department of Chemistry, University of California Berkeley, Berkeley, CA, USA

<sup>2</sup>Climate Change Research Institute, University of New Hampshire, Durham, NH, USA

<sup>3</sup>Department of Chemistry, University of California Irvine, Irvine, CA, USA

<sup>4</sup>NASA Ames Research Center, Moffett Field, CA, USA

<sup>5</sup>Department of Meteorology, Florida State University, Tallahassee, FL, USA

<sup>6</sup>NASA Langley Research Center, Hampton, VA, USA

<sup>7</sup>Department of Earth and Planetary Sciences, University of California Berkeley, Berkeley, CA, USA

\* now at: Chemical Sciences Division, Earth Systems Research Laboratory, National Oceanic and Atmospheric Administration, Boulder, CO, USA

\*\* now at: Cooperative Institute for Research in Environmental Sciences, University of Colorado, Boulder, CO, USA

\*\*\* now at: Department of Chemistry and Biochemistry, University of California, San Diego, La Jolla, CA, USA

Received: 8 October 2009 – Published in Atmos. Chem. Phys. Discuss.: 11 November 2009

Revised: 12 June 2010 – Accepted: 5 July 2010 – Published: 6 August 2010

**Abstract.** Alkyl and multifunctional nitrates ( $\text{RONO}_2$ ,  $\Sigma\text{ANs}$ ) have been observed to be a significant fraction of  $\text{NO}_y$  in a number of different chemical regimes. Their formation is an important free radical chain termination step ending production of ozone and possibly affecting formation of secondary organic aerosol.  $\Sigma\text{ANs}$  also represent a potentially large, unmeasured contribution to OH reactivity and are a major pathway for the removal of nitrogen oxides from the atmosphere. Numerous studies have investigated the role of nitrate formation from biogenic compounds and in the remote atmosphere. Less attention has been paid to the role  $\Sigma\text{ANs}$  may play in the complex mixtures of hydrocarbons typical of urban settings. Measurements of total alkyl and multifunctional nitrates,  $\text{NO}_2$ , total peroxy nitrates ( $\Sigma\text{PNs}$ ),  $\text{HNO}_3$  and a representative suite of hydrocarbons were obtained from the NASA DC-8 aircraft during spring of 2006 in and around Mexico City and the Gulf of Mexico.  $\Sigma\text{ANs}$  were observed to be 10–20% of  $\text{NO}_y$  in the Mexico City plume and to increase in importance with increased photochemical age. We describe three conclusions: (1) Correlations of  $\Sigma\text{ANs}$  with odd-oxygen ( $\text{O}_x$ ) indicate a stronger role for  $\Sigma\text{ANs}$  in the photochemistry of Mexico City than is

expected based on currently accepted photochemical mechanisms, (2)  $\Sigma\text{AN}$  formation suppresses peak ozone production rates by as much as 40% in the near-field of Mexico City and (3)  $\Sigma\text{ANs}$  play a significant role in the export of  $\text{NO}_y$  from Mexico City to the Gulf Region.

## 1 Introduction

The chemistry of alkyl and multifunctional nitrates acts to suppress  $\text{O}_3$  formation in the near field of urban plumes and then to extend the range of ozone formation in the far field by releasing  $\text{NO}_x$  in locations far from  $\text{NO}_x$  emissions (e.g. Ito et al., 2007). However, there are few detailed observational tests capable of assessing the quantitative importance of these effects and current models incorporate contradictory assumptions about elements of the chemistry that are not well constrained by lab or by field observations. Recent analyses of models and their differences (Wu et al., 2007; Ito et al., 2007), field observations (Giacopelli et al., 2005; Farmer and Cohen, 2007; Horowitz et al., 2007; Perring et al., 2009a) and laboratory measurements (e.g. Paulot et al., 2009) have focused attention on the extent to which  $\text{RONO}_2$  molecules preserve the  $-\text{ONO}_2$  functional group upon oxidation. An emerging theme from these papers is that the lifetime of total  $\text{RONO}_2$  (denoted  $\Sigma\text{ANs}$  hereafter), rather



Correspondence to: A. E. Perring  
(anne.perring@noaa.gov)

than the lifetime of any individual  $\text{RONO}_2$  molecule, is the key to understanding the effects of  $\text{RONO}_2$  formation on atmospheric chemistry.

$\Sigma\text{ANs}$  have been observed to be a significant fraction of  $\text{NO}_y$  in a number of different chemical regimes (Day et al., 2003; Rosen et al., 2004; Cleary et al., 2005; Perring et al., 2009a) and have been inferred to be an important photochemical product in Mexico City with potential concentrations of several ppb (Dunlea et al., 2007). Here we present observations of  $\Sigma\text{ANs}$ , measured by thermal dissociation coupled to laser-induced fluorescence detection of  $\text{NO}_2$  (Thornton et al., 2000; Day et al., 2002), in and downwind of Mexico City using the NASA DC-8 platform during the Megacity Initiative: Local and Global Research Observations (MILAGRO) phase of the INTEX-B campaign in the spring of 2006 (Singh et al., 2009; Molina et al., 2010). The aircraft flights targeted plume evolution and crossed the Mexico City plume at its origin and at distances as far as 1000 km downwind. We use these observations to explore the role of  $\Sigma\text{ANs}$  as they affect ozone and nitrogen oxides. We show that  $\Sigma\text{AN}$  chemistry has important consequences for urban  $\text{O}_3$ , for regional photochemistry and for the evolution of  $\text{O}_3$  in the Mexico City plume. We examine aspects of the chemistry that are specific to this plume. We investigate the progression of the  $\text{NO}_y$  distribution as the plume ages with special attention to the continued significance of  $\Sigma\text{ANs}$  as a fraction of  $\text{NO}_y$ .

## 2 Measurements

Observations described here were made aboard the NASA DC-8 during the Intercontinental Transport Experiment-Phase B (INTEX-B), which took place in the spring of 2006. INTEX-B, a NASA-led multi-partner atmospheric chemistry campaign, has been described elsewhere (Singh et al., 2009). One of the stated goals was to investigate the extent and persistence of Mexican pollution outflow as part of the MILAGRO campaign (Molina et al., 2010).

$\text{NO}_2$ ,  $\Sigma\text{PNs}$ , and  $\Sigma\text{ANs}$  were measured using the Berkeley thermal dissociation-laser induced fluorescence instrument (Thornton et al., 2000; Day et al., 2002). Briefly, gas is pulled simultaneously through four channels consisting of heated quartz tubes maintained at specific temperatures for the dissociation of each compound class above. Each heated section is followed by a length of PFA tubing leading to a detection cell where  $\text{NO}_2$  is measured using laser-induced fluorescence. Due to differing X- $\text{NO}_2$  bond strengths,  $\Sigma\text{PNs}$ ,  $\Sigma\text{ANs}$  and  $\text{HNO}_3$  all thermally dissociate to  $\text{NO}_2$  and a companion radical at a characteristic temperature. The ambient channel measures  $\text{NO}_2$  alone, the second channel ( $180^\circ\text{C}$ ) measures  $\text{NO}_2$  produced from the dissociation of  $\Sigma\text{PNs}$  in addition to ambient  $\text{NO}_2$  so the observed signal is  $\text{NO}_2 + \Sigma\text{PNs}$ , the third channel ( $380^\circ\text{C}$ ) measures  $\text{NO}_2 + \Sigma\text{PNs} + \Sigma\text{ANs}$ , and the last channel ( $580^\circ\text{C}$ ) measures

$\text{NO}_2 + \Sigma\text{PNs} + \Sigma\text{ANs} + \text{HNO}_3$ . Concentrations of each class of compound correspond to the difference in  $\text{NO}_2$  signal between two channels set at adjacent temperatures. The difference in  $\text{NO}_2$  signal between the  $180^\circ\text{C}$  and the  $380^\circ\text{C}$  channel, for example, is the  $\Sigma\text{ANs}$  mixing ratio. The instrument deployed for INTEX-B had a heated inlet tip that split in two immediately. Half of the flow was immediately introduced to heated quartz tubes for detection of  $\Sigma\text{ANs}$  and  $\text{HNO}_3$  while the other half was introduced to an additional heated quartz tube for detection of  $\Sigma\text{PNs}$  and an ambient temperature channel for detection of  $\text{NO}_2$ .

Ambient  $\text{NO}_2$  and  $\text{NO}_2$  produced by thermal dissociation was observed by laser-induced fluorescence as described in detail by Thornton et al. (2000). Briefly, a tunable dye laser is pumped at 7 kHz by a Q-switched, frequency doubled  $\text{Nd}^{+3}$  YAG laser. The incoming gas is cooled through the use of a supersonic expansion (Cleary et al., 2002) and the dye laser, utilizing Pyrromethene 597 in isopropanol, is tuned to an isolated rovibronic feature of jet-cooled  $\text{NO}_2$  at 585 nm. The frequency is held for 20 s at the peak of this feature and then for 5 s at an offline position in the continuum absorption. The ratio of peak to off-resonance fluorescence of the chosen feature is 10:1 at 1 atm and the difference between the two signals is directly proportional to the  $\text{NO}_2$  mixing ratio. The laser light is focused in series through two multi-pass (White) cells (discussed in more detail below) and the red-shifted fluorescence is detected using a red-sensitive photomultiplier tube (Hamamatsu). Fluorescence counts are collected at 5 Hz, scattered light at wavelength less than 700 nm is rejected by band-pass filters and time-gated detection is used to eliminate noise resulting from scattered laser light in the cell. We observe a dependence of  $\text{NO}_2$  fluorescence on the external pressure. We calibrate the  $\text{NO}_2$  LIF vs. altitude by direct measurement of  $\text{NO}_2$  from a standard addition during a test-flight. Calibrations were performed at least once every two hours during a level flight leg using a 4.7 ppm  $\text{NO}_2$  reference gas (Praxair) with a stated certainty of  $\pm 5\%$ . The reference gas was compared to a library of standards in lab both before and after the campaign. The individual standards are compared on a regular basis (about every 6 months) to ensure stability and highlight when a given tank has degraded. These standards have been observed to remain stable for up to 5 years and to be accurate at atmospherically relevant mixing ratios to within 1% (Bertram et al., 2005).

The instrument deployed for INTEX-B had two detection cells. The direction of flow into the cell was controlled using a three-way valve and a bypass pump was used to maintain flow in the non-sampled channel. Cell 1 sampled either the ambient (75% of the time) or the  $380^\circ\text{C}$  channel (25% of the time) while cell 2 sampled either the  $180^\circ\text{C}$  (50% of the time) or the  $580^\circ\text{C}$  channel (50% of the time). Thus for every 2 min duty cycle there were three 20 s average measurements of  $\text{NO}_2$ , two 20 s average measurements of  $\Sigma\text{PNs}$ , one 20 s average measurement of  $\Sigma\text{ANs}$ , one 20 s average measurement of  $\text{HNO}_3$  and one 20 s average measurement of the

sum ( $\Sigma\text{PNs} + \Sigma\text{ANs} + \text{HNO}_3$ ). As the  $\Sigma\text{ANs}$  measurement is a subtraction, the uncertainty depends both on  $\Sigma\text{ANs}$  and on the sum ( $\text{NO}_2 + \Sigma\text{PNs}$ ). For example, if there were 100 ppt each of  $\text{NO}_2$  and  $\Sigma\text{PNs}$ , the precision of the  $\Sigma\text{ANs}$  measurement would be  $\sim 15$  ppt in 20 s for  $S/N=2$  at typical laser power and cell alignment. If there were 1 ppb each of  $\text{NO}_2$  and  $\Sigma\text{PNs}$  the precision of the  $\Sigma\text{ANs}$  would be 40 ppt.

We expect to detect both gas and aerosol phase organic nitrates with the TD-LIF instrument because the analogous TD-LIF measurement of  $\text{HNO}_3$  has been shown to be the sum of aerosol and gas-phase  $\text{HNO}_3$  (Fountoukis et al., 2009). While a direct intercomparison of the  $\Sigma\text{ANs}$  measurement has not been published, we have sampled pure standards of ethyl nitrate, propyl nitrate and isoprene nitrates (synthesized by wet chemical methods in the laboratory) in air. In each case we observe signal only in the  $\Sigma\text{ANs}$  channel of the TD-LIF indicating that the nitrates are not dissociating in the other temperature channels. Comparison of TD-LIF observations of an isoprene nitrate standard to observations made using a PTR-MS show both instruments to be consistent to within 10% (Perring et al., 2009b). Comparisons of  $\text{NO}_2$  and  $\Sigma\text{PNs}$  have also been described and indicate similar or better accuracy for these species (Thornton et al., 2003; Fuchs et al., 2010; Wooldridge et al., 2010).

For the present analysis, we use the  $\text{HNO}_3$  measurement made by the University of New Hampshire with a mist chamber followed by ion chromatography (Scheuer et al., 2003; Dibb et al., 2006). This measurement represents the sum of gas-phase  $\text{HNO}_3$  and fine (submicron) aerosol nitrate. Hydrocarbons and  $\text{C}_1$ – $\text{C}_5$  alkyl nitrates were measured by UC Irvine using gas chromatography of whole air samples (Colman et al., 2001). Oxygenated volatile organic carbon species (methyl-ethyl-ketone, methanol, ethanol, acetone and acetaldehyde collectively referred to, when combined with  $\text{CH}_2\text{O}$ , as oxidized volatile organic carbon or OVOC) were measured by NASA Ames using gas chromatography (Singh et al., 1999).  $\text{NO}$  (Georgia Tech) and  $\text{O}_3$  (NASA Langley) were measured through chemiluminescence.  $\text{OH}$  and  $\text{HO}_2$  were measured by laser-induced fluorescence by Penn State (Faloona et al., 2004).  $\text{CH}_2\text{O}$  was measured by NCAR using tunable diode laser absorption spectroscopy (TDLAS) (Fried et al., 2003) and by the University of Rhode Island (URI) using an enzyme-derivatization fluorescence technique following collection in an aqueous medium and high performance liquid chromatographic analysis (Heikes, 1992). There is an unresolved  $\sim 18\%$  discrepancy between the two measurements so we have used an average of the two in the present analysis. URI also employed the enzyme-derivatization fluorescence technique to measure hydrogen peroxide ( $\text{H}_2\text{O}_2$ ).  $\text{CO}$  was measured by differential absorption as described by Sachse et al. (1987).  $\text{NO}_y$  was not measured explicitly but for the purposes of this manuscript we consider it to be the sum of all measured reactive nitrogen species ( $\text{NO}$ ,  $\text{NO}_2$ ,  $\Sigma\text{PNs}$ ,  $\Sigma\text{ANs}$  and  $\text{HNO}_3$ ). Photolysis frequencies are calculated from spectroradiometer measure-

ments as described by Shetter and Muller (1999). Ten-day back trajectories from locations of the DC-8 were calculated using the National Weather Service's Global Forecast Model (GFS) analyses of basic parameters as described by Fuelberg et al. (2007). The GFS data were available at 6 h intervals on a  $1^\circ$  latitude/longitude grid at 64 vertical levels.

The present work uses data from a 1-min merge available at <http://www-air.larc.nasa.gov/missions/intex-b/intexb.html>. We use back trajectories provided with the merged chemical data to select measured air masses that passed within  $\sim 160$  km ( $1.5^\circ$ ) of the T0 site in the center of Mexico City at pressures higher than 680 mbar. The elevation of Mexico City is 2240 m and typical surface pressure is  $\sim 770$  mbar. 680 mbar corresponds to an elevation of about 1 km a.g.l. (above ground level). Considering the 6 local flights out of Houston, there are a total of 2591 trajectories and, of those, 422 satisfy our criteria of having passed through the boundary layer in the vicinity of the Mexico City Metropolitan Area (MCMA).

### 3 Results and analysis

The formation of alkyl and multifunctional nitrates ( $\Sigma\text{RONO}_{2i} \equiv \Sigma\text{ANs}$ ) occurs as a result of reactions between organic peroxy radicals ( $\text{RO}_2$ ) and  $\text{NO}$  (Reaction R1a). The alternative to alkyl nitrate formation is propagation of the radical chain of events, conversion of  $\text{NO}$  to  $\text{NO}_2$ , and subsequent ozone production (Reaction R1b).



The ratio  $k_{1a}/(k_{1a}+k_{1b})$  is  $\alpha$ , the nitrate branching ratio. In this analysis, we examine the concentration of  $\Sigma\text{ANs}$  and the fraction of  $\text{NO}_y$  that is represented by  $\Sigma\text{ANs}$  as a function of time since emission of  $\text{NO}_x$  and VOC at the point of origin in downtown Mexico City. We discuss the evolving relationship between  $\Sigma\text{ANs}$  and  $\text{O}_x$ . Sect. 3.1 we develop a measure of air mass age. In Sect. 3.2 we describe the temporal evolution of  $\text{NO}_y$  partitioning in the plume, in Sect. 3.3 we describe the temporal evolution of the correlation of  $\Sigma\text{AN}$  with  $\text{O}_3$  in the plume.

#### 3.1 Photochemical age

We use the ratio of 2-butyl nitrate ( $\text{CH}_3\text{CHONO}_2\text{CH}_2\text{CH}_3$ ) to butane, an indicator of time since last anthropogenic influence, to sort the MCMA plume points by increasing photochemical age. This indicator of age has been discussed previously by Bertman et al. (1995). Photochemical age indicators depend on the assumption that parent and daughter molecules, in this case a particular straight-chain alkane and its daughter alkyl nitrate arise exclusively from a single chemical reaction (or a chain with a well-defined rate limiting step) and that the loss processes of the daughter are

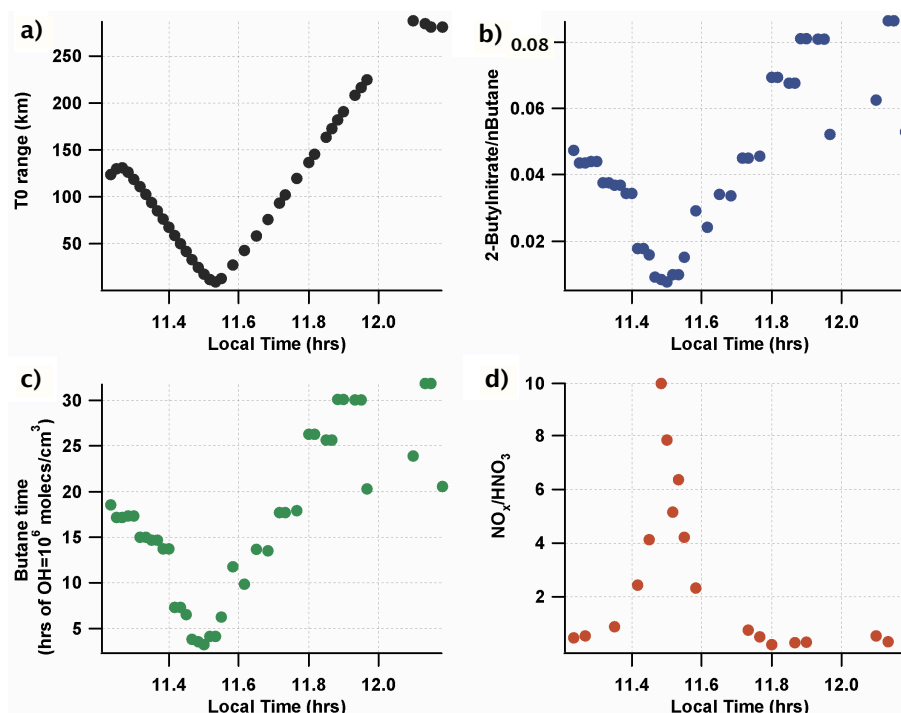


**Fig. 1.** An example from the DC8 Flight #7 of 16 March 2006 of the variation of several indicators of chemical age with distance from the center of Mexico City. Panel (a) shows the distance to Mexico City, panel (b) shows the ratio of 2-butyl nitrate to butane, panel (c) shows the photochemical age inferred from the 2-butyl nitrate/butane ratio and panel (d) shows the ratio of  $\text{NO}_x$  to  $\text{HNO}_3$ .

slower than the parent and well known. In addition, this analysis assumes that the emissions are effectively from a single isolated point source (LaFranchi et al., 2009). Depending on the accuracy required, mixing of a background into the plume must also be taken into account (Day et al., 2003). Neglecting mixing into a constant background doesn't affect the time ordering of the age indicator but does make its absolute magnitude less accurate.

In this case we choose butane and 2-butyl nitrate as the parent-daughter pair. Ages calculated using ratios of 2- and 3-pentyl nitrate to pentane give similar results. Neglecting mixing, and assuming that every  $\text{RO}_2$  formed reacts with  $\text{NO}$ , the change in the concentration of a nitrate over time is then:

$$\frac{d[\text{RONO}_2]}{dt} = \alpha k_A [\text{RH}] - k_B [\text{RONO}_2] \quad (1)$$

where  $\alpha$  is the nitrate branching ratio,  $k_A = k_{\text{OH}+\text{RH}} \cdot [\text{OH}]$  and  $k_B = k_{\text{OH}+\text{RONO}_2} \times [\text{OH}] + J_{\text{RONO}_2}$ . The parameters for butane and 2-butyl nitrate are taken from Bertman et al. (1997):  $k_{\text{OH}+\text{Butane}} = 2.54 \times 10^{-12} \text{ cm}^3/\text{molecule/s}$ ,  $k_{\text{OH}+2\text{Butylnitrate}} = 9.2 \times 10^{-13} \text{ cm}^3/\text{molecule/s}$ ,  $\alpha = 0.077$  and  $J_{2\text{Butylnitrate}} = 1.1 \times 10^{-6} \text{ s}^{-1}$ . For the present calculation we have assumed  $\text{OH} = 3 \times 10^6 \text{ molecules/cm}^3$ , a reasonable daytime average concentration for the core of the Mexico City urban plume. Dusanter et al. (2009) report midday  $\text{OH}$  concentrations of  $7\text{--}8 \times 10^6 \text{ molecules/cm}^3$  in downtown Mexico City and median concentrations observed aboard

the DC8 for back trajectories tracing to Mexico City ranged from  $\sim 8 \times 10^6 \text{ molecules/cm}^3$  within the Mexico City Basin to  $\sim 4 \times 10^6 \text{ molecules/cm}^3$  over the Gulf of Mexico.

The above equation integrates to:

$$\frac{[\text{RONO}_2]}{[\text{RH}]} = \frac{\alpha k_A}{(k_A - k_B)} \left( 1 - e^{(k_A - k_B)t} \right) - \frac{[\text{RONO}_2]_0}{[\text{RH}]_0} e^{(k_A - k_B)t} \quad (2)$$

If we assume  $[\text{RONO}_2]_0 = 0$  and solve for  $t$  we find:

$$t = \frac{\ln \left( 1 - \frac{[\text{RONO}_2]}{[\text{RH}]} \frac{(k_B - k_A)}{\alpha k_A} \right)}{(k_A - k_B)} \quad (3)$$

Bertman et al. (1995) showed that these assumptions were adequate for evolving airmasses observed at Scotia Pennsylvania and the Kinterbish Wildlife Area, Alabama when applied to nitrates derived from hydrocarbons larger than propane.

Figure 1 shows the distance from T0 (panel a), the observed ratio of 2-butyl nitrate to butane (panel b), the age calculated from the 2-butyl nitrate to butane ratio (panel c) and the observed  $\text{NO}_x$  to  $\text{HNO}_3$  ratio (panel d) from a segment of the DC8's flight of 16 March 2006. The  $\text{NO}_x$  to  $\text{HNO}_3$  ratio, which has also been widely employed as an indicator of photochemical processing, is expected to decrease with increased age as long as oxidation of  $\text{NO}_2$  is more rapid than

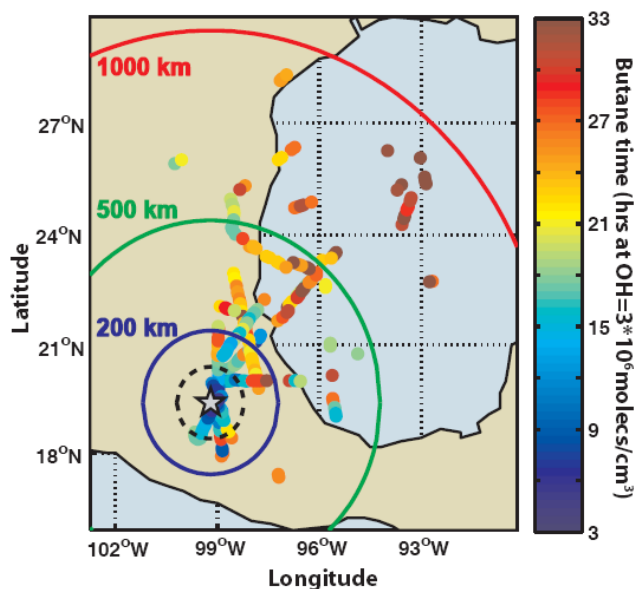


**Fig. 2.** Locations of data that trace back to the region around Mexico City colored by their photochemical age in hours of processing at  $\text{OH}=3\times 10^6$  molecules/ $\text{cm}^3$ . The black star represents the location of Mexico City and the dashed black circle shows the limit of the region we have defined as the Mexico City Area (within 100 km of the city center). The colored circles represent distances from the center of Mexico City of 200 km (blue), 500 km (green) and 1000 km (red).

deposition of  $\text{HNO}_3$ . Figure 2 shows the calculated age of all points that have back trajectories that trace back to Mexico City and Fig. 3 shows the relationship between the calculated age for these points and the distance to the T0 site in downtown Mexico City. Although we use a single value for OH in these calculations, it should also be noted that the rate of photochemical aging slows as the plume becomes more dilute and the OH concentration decreases. The OH concentration drops by more than a factor of 2 between the center of Mexico City and the Gulf of Mexico and this drives the shape of the curve shown in Fig. 3.

Much of the spread in the relationship between photochemical age and distance to the T0 site can be explained by variation in wind velocity. For example, the average measured wind velocity below 4 km altitude (where most of the plume sampling occurred) on 16 March was  $\sim 5.5$  m/s (blue points) while that on 19 March was  $\sim 10$  m/s (red points). The higher wind velocity on 19 March carried the air mass farther from the source at equivalent photochemical aging than the mean. Note that the choice of OH concentration of  $3\times 10^6$  molecules/ $\text{cm}^2$  gives photochemical ages in the first two days of plume evolution that are similar to the transport times calculated from observed wind speeds; i.e. on the day with a windspeed of 5.5 m/s the calculated photochemical age of the points near 1000 km is  $\sim 45$  h while the transport time would be  $\sim 50$  h. Additional spread in the transport

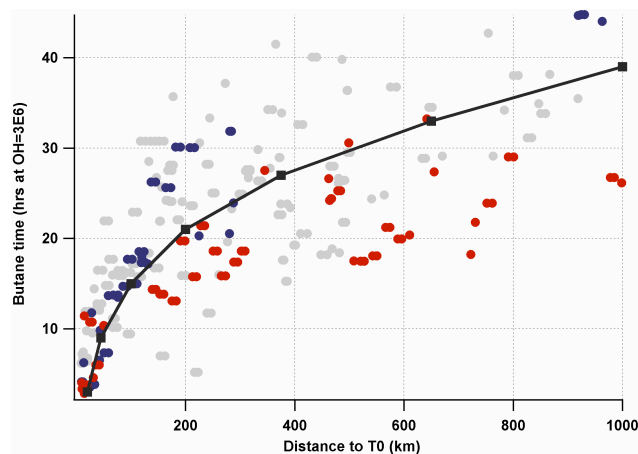


**Fig. 3.** The relationship between the age calculated from the ratio of 2-butyl nitrate to n-butane and the distance to the T0 site in the center of Mexico City. Gray points show all data that traces back to Mexico City, red points represent DC-8 Flight 7 and blue points represent DC-8 Flight 8, two flights for which the average wind speed varied widely as discussed in the text. The black line represents a qualitatively typical relationship.

time-photochemical time relationship is also introduced as a result of using a photochemical clock that turns off at night.

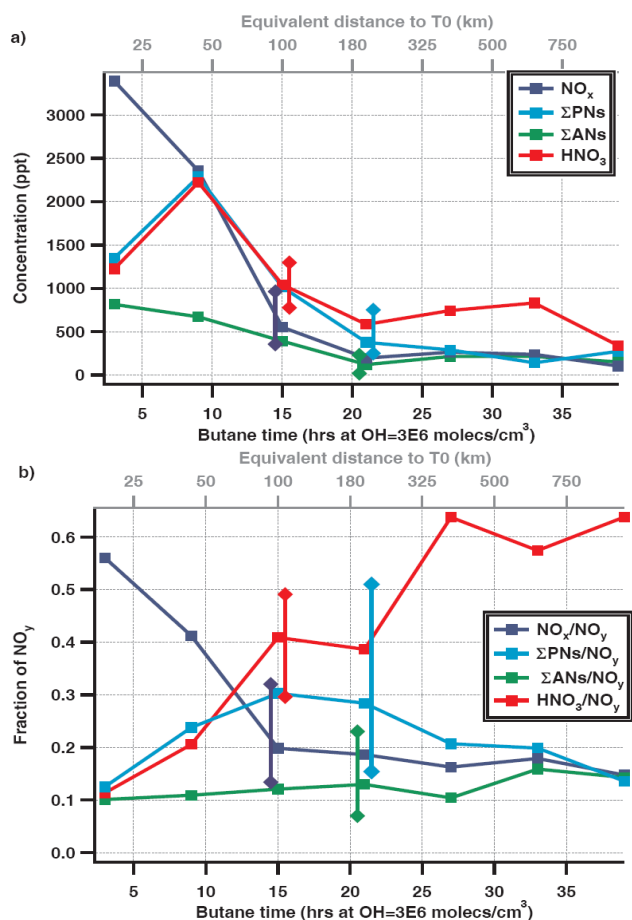
### 3.2 $\text{NO}_y$ speciation in the Mexico City Plume

Figure 4a shows concentrations of the components of  $\text{NO}_y$  as a function of photochemical age and 4b shows  $\text{NO}_y$  speciation as a function of photochemical age. Near Mexico City (time  $< 6$  h)  $\text{NO}_x$  is  $\sim 3.5$  ppb and the dominant component of  $\text{NO}_y$ . Within 200 km (by  $\sim 20$  h)  $\text{NO}_x$  decreases to  $< 25\%$  of  $\text{NO}_y$  and at the longest time considered (130 h)  $\text{NO}_x$  is 15% of  $\text{NO}_y$ , comparable to  $\Sigma\text{PNs}$  and  $\Sigma\text{ANs}$ .  $\text{HNO}_3$  is a minor fraction of  $\text{NO}_y$  (10%) close to Mexico City and increases to  $\sim 60\%$  at the longest times.

The concentration of  $\Sigma\text{PNs}$  peaks at  $\sim 8$  h and  $\Sigma\text{PNs}$  as a fraction of  $\text{NO}_y$  peak at  $\sim 15$  h (100 km) where they account for 30% of  $\text{NO}_y$  after which they decrease to about  $\sim 15\%$  of  $\text{NO}_y$  at  $\sim 40$  h. Qualitatively this is the expected pattern. Previous analyses have shown that net production of peroxy nitrates occurs in the near-field of source regions where concentrations of  $\text{NO}_2$  and  $\text{RO}_2$  are high and the formation rate exceeds the rate of thermal decomposition. As the plume becomes more dilute, the formation rate will decrease exponentially while the thermal decomposition rate is determined only by the temperature. For urban plumes that experience rapid lofting and wet removal of both  $\text{HNO}_3$  and  $\Sigma\text{ANs}$ ,  $\Sigma\text{PNs}$  become the dominant  $\text{NO}_y$  reservoir in the colder, lofted air mass (Altshuller, 1993; Singh and Salas, 1989; Talbot et al., 2003). The Mexico City Plume, as selected based on the criteria described above, was encountered exclusively below 5 km. The plume was almost entirely

**Table 1.** Column 1 identifies the hydrocarbons and columns 2 and 3 show OH rate constants and nitrate branching ratios for the suite of hydrocarbons observed in Mexico City. Columns 4–6 show the median concentrations and the associated ozone and alkyl nitrate production rates respectively.

	$k_{\text{OH}}$ ( $\text{cm}^2 \text{ molecule}^{-1} \text{ s}^{-1}$ )	$\alpha$	Concentration (ppt)	$P(\text{O}_3)$ (ppt/hr)	$P(\text{ANs})$ (ppt/hr)
Alkanes					
Methane	6.34E-15	0.001	1 969 000	701	0.35
Ethane	2.58E-13	0.009	2966	43	0.19
Propane	1.10E-12	0.036	20 697	1279	23.01
nButane	2.54E-12	0.083	8022	1144	47.49
nPentane	4.00E-12	0.123	1809	406	24.99
iButane	2.19E-12	0.027	2553	314	4.24
iPentane	3.90E-12	0.075	3625	794	29.77
2-Methylpentane	5.30E-12	0.111	1004	299	16.59
3-Methylpentane	5.40E-12	0.109	628	190	10.38
Hexane	5.45E-12	0.212	753	230	24.43
Heptane	7.02E-12	0.278	217	86	11.89
Octane	8.71E-12	0.346	109	53	9.22
Nonane	9.99E-12	0.393	54	30	5.95
Decane	1.12E-11	0.417	54	34	7.08
Alkenes					
Ethene	8.20E-12	0.0005	3999	1842	0.46
Propene	2.63E-11	0.021	432	638	6.70
1-Butene	3.14E-11	0.039	73	129	2.51
Butadiene	6.66E-11	0.065	5	19	0.61
Isoprene	1.01E-10	0.07	23	130	4.57
Methylpropene	5.14E-11	0.012	45	130	0.78
2-Methyl 1-butene	6.07E-11	0.02	45	153	1.53
3-Methyl 1-butene	3.18E-11	0.059	11	20	0.58
2-Methyl 2-butene	8.69E-11	0.034	34	166	2.82
trans 2-Butene	6.40E-11	0.041	51	183	3.76
cis 2-Butene	5.64E-11	0.041	30	95	1.95
1-Pentene	3.14E-11	0.059	49	86	2.55
trans 2-Pentene	6.70E-11	0.064	42	158	5.06
cis 2-Pentene	6.50E-11	0.064	18	66	2.10
Aromatics					
Benzene	1.22E-12	0.029	851	58	0.85
Ethylbenzene	7.00E-12	0.072	290	114	4.10
Propylbenzene	5.80E-12	0.093	39	13	0.59
Toluene	5.96E-12	0.079	3805	1274	50.31
3-Ethyltoluene	1.86E-11	0.094	86	90	4.22
4-Ethyltoluene	1.18E-11	0.137	34	23	1.54
O-Xylene	1.36E-11	0.081	197	150	6.09
M-Xylene	2.30E-11	0.074	250	323	11.95
P-Xylene	1.43E-11	0.097	141	113	5.49
1,3,5-Trimethylbenzene	5.76E-11	0.127	5	16	1.03
1,2,4-Trimethylbenzene	3.25E-11	0.105	93	170	8.91
Other					
CO	2.39E-13	0	600000	4027	0.00
H <sub>2</sub> CO	8.37E-12	0	7793	1832	0.00
Acetaldehyde	1.58E-11	0	2497	2216	0.00
Acetone	1.79E-13	0	2306	25	0.00
Methanol	9.11E-13	0	3542	194	0.00
Ethanol	3.27E-12	0	978	192	0.00
Methylethylketone	1.15E-12	0	305	21	0.00
Total				20 268	347



**Fig. 4.** (a) Observed concentrations of the components of  $\text{NO}_y$  as a function of photochemical age. Error bars show the  $1\sigma$  variation in the data. (b) Observed fraction of  $\text{NO}_y$  comprised of each of the  $\text{NO}_y$  reservoirs as a function of photochemical age. Again, error bars show the variation at  $1\sigma$ .

(95%) at temperatures above 280 K corresponding to a PAN thermal lifetime of less than 10 h.  $\Sigma\text{ANs}$  start at 10% of  $\text{NO}_y$  near Mexico City. At the longest time they are of comparable importance to  $\Sigma\text{PNs}$  (~15% of  $\text{NO}_y$ ). If  $\Sigma\text{ANs}$  react and release  $\text{NO}_2$ , they may be important in the redistribution of reactive nitrogen within the Gulf of Mexico.

We can account, at least partially, for dilution by comparing enhancements over the background to CO, which is a conserved tracer on the timescale of this plume study. CO is lost to reaction with OH at a rate of approximately 6% per day. Photochemical production of CO is also minimal on these timescales. We calculate that, over 40 h of photochemical aging at our assumed OH concentration, 2.6 ppb of CO would be produced from methane oxidation and an additional 3–4 ppb would be produced from oxidation of formaldehyde, acetone and ethane (using concentrations of each observed in Mexico City). Oxidation of larger hydrocarbons is likely to contribute primarily through the production of formaldehyde which we account for above. For comparison, CO decreases

from 600 ppb at 0–5 h photochemical age to 450 ppb at about 10 h and is mixing into a background of 132 ppb CO. The expected CO production is less than 2% of the observed decrease in concentration over 40 h of photochemical aging and the decay in CO is therefore primarily a measure of dilution. Molecules that decay faster than CO can be considered to be removed by chemistry or deposition while those that decay more slowly are being produced in the plume.

Figure 5a shows fractional enhancement over the background for  $\text{NO}_y$ , CO,  $\text{NO}_x$ ,  $\Sigma\text{PNs}$  and  $\Sigma\text{ANs}$ . The fractional enhancement over background for species  $X$  is defined as:

Fractional enhancement of species  $X$

$$= (X - X_{\text{background}}) / (X_{\text{initial}} - X_{\text{background}})$$

where  $X_{\text{initial}}$  is the mean observed concentration of species  $X$  at less than 10 h of photochemical aging and  $X_{\text{background}}$  is the mean observed concentration of species  $X$  at the longest photochemical ages over the Gulf of Mexico. Background concentrations used were 132 ppb for CO, 1.22 ppb for  $\text{NO}_y$  and as shown in Fig. 4a for the different  $\text{NO}_y$  species. The near identical fractional dilutions of  $\text{NO}_y$  and CO indicates that the airmasses were not subject to large depositional losses, consistent with the fact that the plume was primarily encountered between 2 and 4 km and should have been connected to the planetary boundary layer weakly if at all. Figure 5b shows the fractional enhancement of the components of  $\text{NO}_y$  divided by the fractional enhancement of CO, which should effectively cancel out the effect of dilution and allow us to examine the effect of chemistry.  $\Sigma\text{PNs}$ , which are primarily produced within the first 15 hrs of plume evolution, are depleted relative to CO throughout the plume.  $\text{NO}_x$  is initially enhanced relative to CO because net dissociation of  $\Sigma\text{PNs}$  is a source of  $\text{NO}_x$ . In the most aged airmasses considered,  $\text{NO}_x$  is depressed relative to CO because it has been converted to  $\text{HNO}_3$ .  $\text{HNO}_3$  is chemically produced in the plume and thus lies above the dilution line.  $\Sigma\text{ANs}$  behave similarly to  $\text{HNO}_3$  confirming that they, too, continue to be produced as the plume ages although most of the production occurs early in the plume. The lines all converge at the longest photochemical age because that is what we have defined as “background” conditions.

### 3.3 The evolution of the relationship between $\Sigma\text{ANs}$ and $\text{O}_x$

Since  $\text{O}_x$  ( $\text{O}_x = \text{O}_3 + \text{NO}_2$ ) and  $\Sigma\text{ANs}$  arise from alternative channels of Reaction (R1) the slope of the correlation of  $\text{O}_x$  and  $\Sigma\text{ANs}$  is a measure of the balance between chain propagation ( $\text{O}_x$  production) and termination ( $\Sigma\text{ANs}$  production) as long as losses of both are slow relative to production. This assumption will be investigated in more detail in Sect. 4.2. Lower slopes imply a more significant role for  $\Sigma\text{ANs}$  formation. Figure 6 shows the observed correlation between  $\text{O}_x$  and  $\Sigma\text{ANs}$  at a range of photochemical ages less than 5 h

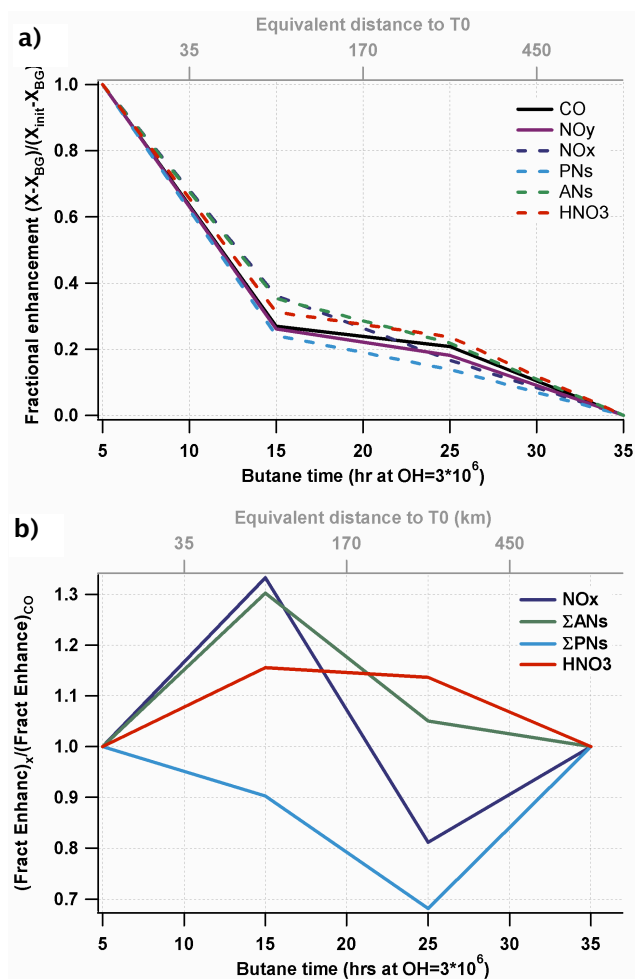


**Fig. 5.** (a) Fractional enhancement of CO (black solid), NO<sub>y</sub> (purple solid), NO<sub>x</sub> (dotted dark blue), ΣPNs (dotted cyan), ΣANs (dotted green) and HNO<sub>3</sub> (dotted red) used to assess possible impacts of deposition. Background levels are assumed to be equal to levels observed at the most aged point. The overall change is the change from the least aged to most aged points. See text for more description. (b) Dilution of the various NO<sub>y</sub> reservoirs relative to CO defined as (Fractional enhancement of X)/(Fractional enhancement of CO). NO<sub>x</sub> is shown in dark blue, ΣPNs in light blue, ΣANs in green and HNO<sub>3</sub> in red.

in red and at greater than 35 h in blue. The slope observed in the fresh plume (17 O<sub>x</sub>/ΣAN) and the more aged plume (90 O<sub>x</sub>/ΣAN) are shown by the solid lines. The dotted lines represent the slopes observed at intermediate age ranges (10–20 h, 20–30 h and 30–40 h) and show a gradual increase over time. The y-intercepts for the fits obtained for different photochemical ages are all similar (52.5±2.5 ppb O<sub>x</sub>). It is therefore reasonable to assume a constant background for mixing with ΣAN levels that are low (0–50 ppt) and O<sub>x</sub> that is 50–55 ppb. If the whole plume is being diluted into the same background mixture, then dilution will impact the observed concentrations of O<sub>x</sub> and ΣANs but not affect the slope of the correlation.

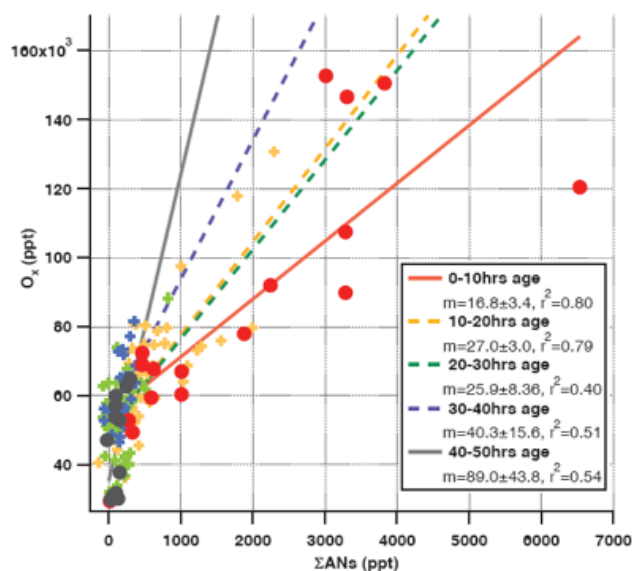


**Fig. 6.** Observed slopes of ΣANs v. O<sub>x</sub> throughout the plume. The freshest points (photochemical age 0–10 h) are shown by red circles and the most aged points (photochemical age >40 h) are shown by gray circles. Data from intermediate ages are shown as colored crosses. Lines show the best fits obtained for each age range and slopes are reported along with the 1 σ confidence intervals and r<sup>2</sup> values for each of the fits.

The change in slope with time indicates a variable role for ΣAN production over the lifetime of the plume. Slopes of O<sub>x</sub>/ΣANs have been reported for a number of different locations using ground-based ΣAN measurements at UC-Blodgett Forest Research Center (Day et al., 2003), Granite Bay CA (Cleary et al., 2005), Houston, TX (Rosen et al., 2004), the Big Hill field site in the Sierra Foothills (Murphy et al., 2006) and using airborne measurements made over the southeastern US aboard the NASA DC-8 (Perring et al., 2009a). Typically lower ΣANs v. O<sub>x</sub> slopes are observed in urban locations than in more rural ones. For comparison with the current dataset, Rosen et al. (2004) found a slope of 29 O<sub>x</sub>/ΣANs in the morning in Houston which increased to 41 in the afternoon and the average afternoon slope that we observed at the T1 site in Mexico City during MILAGRO was 22. Levels of ΣANs in remote areas of the troposphere have been observed to be very low and observed O<sub>x</sub>/ΣANs slopes in the remote Pacific are found to be 200–500. This is higher than the slope found for even the longest times considered in the present analysis and illustrates the fact that the Mexico City plume impacts much of the Gulf region.

The instantaneous production rates of O<sub>x</sub> and ΣANs are given by:

$$P(\text{O}_x)_{\text{inst}} = \sum_i \gamma_i (1 - \alpha_i) k_{\text{OH}+\text{RH}_i} [\text{OH}] [\text{RH}_i] \quad (4)$$

$$P(\Sigma\text{ANs})_{\text{inst}} = \sum_i \alpha_i k_{\text{OH}+\text{RH}_i} [\text{OH}] [\text{RH}_i] \quad (5)$$



where  $\alpha_i$  is the nitrate branching ratio for  $\text{RH}_i$  and  $\gamma_i$  is the immediate number of  $\text{O}_3$  produced from the oxidation of  $\text{RH}_i$ .  $\gamma$  is equal to 2 for most hydrocarbons since Reaction (R1b) typically results in the net production of 2  $\text{O}_3$  molecules; one from photolysis of the  $\text{NO}_2$  formed directly from  $\text{RO}_2+\text{NO}$  and a second when subsequent alkoxy radical decomposition forms  $\text{HO}_2$  and that  $\text{HO}_2$  oxidizes  $\text{NO}$  to  $\text{NO}_2$  followed by photolysis of that  $\text{NO}_2$ . See Rosen et al. (2004) for a more complete discussion of these equations. The variable slopes observed in the plume are the result of the integrated instantaneous production rates. While there is no simple analytical expression for the integrated production, in what follows we use the instantaneous production rates to assess whether we can explain the changes in the slope from point to point throughout the plume.

Taking the ratio of the two instantaneous production rates above we can find the relationship between the observed slope and the average branching ratio of the VOC mixture given by:

$$\frac{P(\text{O}_3)}{P(\Sigma\text{ANs})} \equiv \frac{\bar{\gamma}(1-\bar{\alpha})}{\bar{\alpha}} \approx \frac{2-2\bar{\alpha}}{\bar{\alpha}} \quad (6)$$

where ( $\bar{\alpha}$ ) is the average branching ratio. A slope of 60  $\text{O}_x/\Sigma\text{AN}$  for example, implies ( $\bar{\alpha}$ )=3.2% while a slope of 20 implies ( $\bar{\alpha}$ )=9.1%.

We can also calculate the production rate of  $\text{O}_x$  and  $\Sigma\text{ANs}$  based on known or assumed reaction rates and nitrate formation branching ratios as given by the Leeds Master Chemical Mechanism (MCM). Table 1 summarizes the values of  $\alpha$  and  $k_{\text{OH}}$  used in this analysis, the median concentrations of each VOC as observed within 5 h of Mexico City and the associated instantaneous production rates for  $\text{O}_3$  and  $\Sigma\text{ANs}$ . The calculated instantaneous  $\text{O}_x/\Sigma\text{ANs}$  slope for each point is the ratio of the total  $P(\text{O}_x)$  (column 5) to the total  $P(\Sigma\text{ANs})$  (column 6). The calculated slope from Table 1 (for data within 5 h of Mexico City) is then 20 268/347, which is approximately 60  $\text{O}_x/\Sigma\text{AN}$ . Parallel calculations are performed for each of the different ranges of plume age. In addition to the 30 hydrocarbon species measured on-board the DC8, we have estimated concentrations of another 12 which are marked in the table by bold italic font with underlining. The nine unmeasured alkenes were estimated based on correlations with 1-butene observed at the T1 site. The three long-chain alkanes were estimated based on correlations with n-heptane observed in Houston. Observations described in Parrish et al. (2009) and others show that emission ratios of related hydrocarbons (as inferred from observed hydrocarbon ratios) vary little from city to city even though emission rates vary dramatically. The estimated compounds add ~5% to  $P(\text{O}_3)$  and 13% to  $P(\Sigma\text{ANs})$ . Note also that we have not included  $\Sigma\text{ANs}$  themselves as precursor molecules in the initial calculations, as has been done previously (Rosen et al., 2004; Cleary et al., 2005). The specific molecular structure of the nitrates will determine both their OH reactivities and di-nitrate branching ratios and the extreme variation in possi-

ble values for both of these parameters in the evolving plume makes them hard to approximate with a single value.

## 4 Discussion

### 4.1 $\Sigma\text{ANs}$ sources in Mexico City

The large  $\bar{\alpha}$  (10.5%) implied by the 16.8  $\text{O}_x/\Sigma\text{ANs}$  slope observed in and around Mexico City indicates a significant role for  $\Sigma\text{ANs}$  in the photochemistry of the region.  $\Sigma\text{AN}$  formation at such high ( $\bar{\alpha}$ ) has a strong influence on  $\text{O}_3$  formation rates because  $\text{RONO}_2$  formation is competitive with  $\text{HNO}_3$  formation as a chain termination reaction for  $\text{HO}_x$  and  $\text{NO}_x$  catalytic cycles. Given this large influence it would be valuable to understand the  $\Sigma\text{AN}$  source molecules in detail. There are large differences between the observed (17) and calculated (60)  $\Sigma\text{ANs}$  v.  $\text{O}_x$  slope near Mexico City, which implies the existence of unexplained photochemistry. This could be due to a combination of (1) the presence of unmeasured compounds with large nitrate branching ratios, (2) underestimates of currently accepted branching ratios for measured compounds, (3) a large component of di-nitrate formation from  $\Sigma\text{ANs}$  (which would produce 2 molecules of  $\text{NO}_2$  in the TD-LIF).

Before further evaluation of these options it is useful to develop an independent check on the inferred  $\alpha$ . One such independent check is to compare the observed ratio of  $\Sigma(\text{C}_1\text{--C}_5 \text{ nitrates})/\Sigma\text{ANs}$  to the ratio calculated from the instantaneous production rate given by Eq. (5). Namely:

$$\left(\frac{\Sigma(\text{C}_1\text{--C}_5 \text{ nitrates})}{\Sigma\text{ANs}}\right)_{\text{calc}} \approx \frac{\left(\sum_{j=\text{C1}}^{\text{C5}} \alpha_j \times k_{\text{OH}+\text{RH}_j} \times \text{RH}_j\right)}{\left(\sum_i \alpha_i \times k_{\text{OH}+\text{RH}_i} \times \text{RH}_i\right)} \quad (7)$$

where  $\alpha_j$  and  $k_{\text{OH}+\text{RH}_j}$  are reported branching ratios and OH rate constants for only the hydrocarbon precursors to the  $\text{C}_1\text{--C}_5$  nitrates measured by GC and  $\alpha_i$  and  $k_{\text{OH}+\text{RH}_i}$  are reported or estimated branching ratios and OH rate constants for the entire suite of observed and estimated hydrocarbons given in Table 1.  $\Sigma(\text{C}_1\text{--C}_5 \text{ nitrates})$  are predicted to be 27% of  $\Sigma\text{ANs}$  in Mexico City based on the relative production rates but they were only observed to be 10%. As with the discrepancy between calculated and observed  $\Sigma\text{ANs}$  v.  $\text{O}_x$  slopes, this indicates an underestimate of  $\Sigma\text{AN}$  production. We should also note that, similar to the analysis performed above regarding the relative production of  $\text{O}_x$  and  $\Sigma\text{ANs}$ , we have assumed that the loss rates of both  $\text{C}_1\text{--C}_5$  nitrates and  $\Sigma\text{ANs}$  are slow relative to production. The lifetimes of the simple  $\text{C}_1\text{--C}_5$  nitrates are well constrained by both laboratory and field measurements with typical photolysis lifetimes of ~13 days (2-pentyl nitrate) to 10 days (methyl nitrate) and lifetimes to oxidation by OH (at  $\text{OH}=3 \times 10^6$ ) of 2 days (2-pentyl nitrate) to ~130 days (methyl nitrate). We calculate an overall loss rate of 2.7 ppt/h for  $\text{C}_1\text{--C}_5$  nitrates in Mexico City (as compared

to an instantaneous production rate of 31 ppt/h). At (15 h, 35 h) we calculate an instantaneous production rate of (2.7, 0.5) ppt/h and a loss rate of (0.65, 0.4) ppt/h. The lifetime of  $\Sigma\text{ANs}$  as a class of compounds is more difficult to determine as the exact lifetime of any particular alkyl or multifunctional nitrate will depend on the specific structure. As a first guess we can make the approximation that, on average, they have an OH rate constant similar to that of toluene (a molecule with a moderately reactive double bond), that 20% of the reactions with OH lead to loss of nitrate functionality and release of  $\text{NO}_2$  (as opposed to creating a more functionalized nitrate) and that the photolysis rate is similar to n-pentyl nitrate (one of the larger and shorter-lived nitrates for which we have a well-characterized photolysis lifetime). We then calculate a loss rate of 13.6 ppt/h in Mexico City, 1.6 ppt/h at 500 km and 1.3 ppt/h at 1000 km as compared to production rates of 638, 66 and 14 ppt/h at 0, 500 and 1000 km respectively.

The analyses described above examining the production rate of  $\Sigma\text{ANs}$  relative to both  $\text{O}_x$  and  $\text{C}_1\text{--C}_5$  nitrates lead to remarkably similar conclusions. As outlined previously, the slope (17) of the correlation between  $\Sigma\text{ANs}$  and  $\text{O}_x$  observed in Mexico City implies an average branching ratio for nitrate formation of 10.5%. In contrast, the average branching ratio for nitrate formation calculated from current chemical mechanisms is 3.2% and the  $\text{O}_x/\Sigma\text{ANs}$  correlation implies that the rate of  $\Sigma\text{ANs}$  production is 3.3 times higher than expected. In corroboration, the observed fraction of  $\Sigma\text{ANs}$  comprised of  $\text{C}_1\text{--C}_5$  nitrates is 10% rather than the expected 27% implying that  $\Sigma\text{ANs}$  production is 2.7 times higher than expected. Below we examine some possible explanations for the higher-than-expected  $\Sigma\text{ANs}$  production rate.

First we consider the possibility of unmeasured nitrate precursors. A large burden of long-chain ( $>\text{C}_{10}$ ) alkanes has been proposed based on observations of SOA in large urban centers and analysis of diesel exhaust (Robinson et al., 2007). Since long-chain alkanes have high nitrate formation branching ratios ( $\sim 35\%$ ), adding them to our inventory could bring the observed and calculated branching ratios into agreement. A concentration of 0.5 ppb of a compound that reacted gas-kinetically with OH and had a branching ratio of 35% would result in a calculated  $\text{O}_x/\Sigma\text{ANs}$  slope near Mexico City of 25  $\text{O}_x/\Sigma\text{AN}$  (compared to the observed value of 17) and a calculated  $\Sigma(\text{C}_1\text{--C}_5 \text{ nitrate})/\Sigma\text{ANs}$  ratio of 8% (compared to the observed value of 10%).

A second possible explanation is that current estimates of nitrate branching ratios for some compounds that were measured are too low. Most notably, Mexico City is observed to have a large burden of aromatic compounds and there currently exists no aromatic oxidation experiment in the presence of  $\text{NO}_x$  that has shown carbon closure. The nitrate branching ratios used here are those used in MCM which are estimated using an expression proposed by Carter and Atkinson (1989). The full implementation of the MCMv3.1 aromatic oxidation scheme is described by Bloss et al. (2005).

In addition to uncertainty in the yield of nitrates from the initial oxidation of aromatic compounds, there is a high degree of uncertainty in the yields of ring-opening vs. ring-retaining products (Hamilton et al., 2003; Jenkin et al., 2003; Wagner et al., 2003; Wyche et al., 2009). The products of ring-opening pathways could themselves have high nitrate yields and significant nitrate formation could thus result from oxidation of the first-generation products of aromatic oxidation. A doubling of the nitrate branching ratio for all aromatic compounds would decrease the calculated  $\Sigma\text{ANs}$  v.  $\text{O}_x$  slope to 39 and the calculated  $\Sigma(\text{C}_1\text{--C}_5 \text{ nitrates})/\Sigma\text{ANs}$  ratio to 22% which is an improvement. While uncertainties in nitrate formation from aromatic compounds alone are unlikely to bring the calculations and observations into complete agreement, nitrate formation from aromatics and their oxidation products is significant in Mexico City and further study is warranted.

The third possibility is that  $\Sigma\text{ANs}$  themselves are the unaccounted-for nitrate precursors. As noted above, they were not included in the initial calculation due to uncertainties in rate constants and branching ratios but it is highly likely that there is appreciable di-nitrate formation in the chemical environment of Mexico City. The calculations performed for datasets in Granite Bay and Houston assumed an OH rate constant of  $1.6 \times 10^{-11}$  molec/cm<sup>3</sup>/s and a branching ratio of 5%. If we include  $\Sigma\text{ANs}$  in the calculation here using these parameters, the calculated  $\Sigma\text{ANs}$  v.  $\text{O}_x$  slope and  $\Sigma(\text{C}_1\text{--C}_5 \text{ nitrates})/\Sigma\text{ANs}$  ratio are minimally changed. However, many of the 1st generation nitrates in Mexico City should be large molecules that retain at least one double bond. They may therefore react relatively quickly with OH and should have reasonably high branching ratios. If we assume that they have an OH rate constant of  $7 \times 10^{-11}$  cm<sup>3</sup>/molec/s, comparable to estimates of OH rate constants for isoprene nitrates (Perring et al., 2009a; Giapopelli et al., 2005) and a branching ratio of 17%, then the calculated  $\Sigma\text{ANs}$  v.  $\text{O}_x$  slope is 25 and the calculated  $\Sigma(\text{C}_1\text{--C}_5 \text{ nitrates})/\Sigma\text{ANs}$  ratio is 0.08 which is comparable agreement to that achieved by the addition of 0.5 ppb of unmeasured long-chain hydrocarbons.

We should also note that the nighttime reaction of  $\text{NO}_3$  with alkenes is known to give rise to  $\Sigma\text{ANs}$  production without associated  $\text{O}_3$  production (Warneke et al., 2004). The nitrate formation rate from  $\text{NO}_3$ -initiated oxidation is typically much higher than for OH-initiated oxidation and this reaction could represent a significant source of  $\Sigma\text{ANs}$ . Based on concentrations of  $\text{NO}$ ,  $\text{NO}_2$  and  $\text{O}_3$  observed at the T1 site in the hours before sunset (medians of 1 ppb, 8.6 ppb and 63 ppb respectively) and a nighttime temperature of 10 °C, we calculate a possible total combined  $\text{NO}_3$  and  $\text{N}_2\text{O}_5$  (an  $\text{NO}_3$  reservoir species) production of 1.4 ppb over the course of a typical night. Therefore, even if all of the available  $\text{NO}_3$  were to react with alkenes with a 70% nitrate yield, it would lead to a maximum production of 1 ppb of  $\Sigma\text{ANs}$  which is  $\sim 20\%$  of observed daytime concentrations and would perturb the

$\text{O}_x/\Sigma\text{ANs}$  slope by a similar amount, far smaller than the observed discrepancy. In addition, significant nighttime concentrations (100's of ppt) of NO were observed at the T1 site at night, presumably due to local NO emissions. NO emissions would inhibit the accumulation of appreciable concentrations of  $\text{NO}_3$  by titration. If we instead calculate potential  $\text{NO}_3$  and  $\text{N}_2\text{O}_5$  production based on median concentrations of NO,  $\text{NO}_2$  and  $\text{O}_3$  observed aboard the NASA DC-8 (0.4 ppb, 1.2 ppb and 68 ppb respectively), the potential production is much smaller ( $\sim 110$  ppt). It is therefore likely that typical nighttime concentrations of  $\text{NO}_3$  and  $\text{N}_2\text{O}_5$  are substantially lower than the possible 1.4 ppb calculated above and that  $\Sigma\text{ANs}$  production from  $\text{NO}_3$  oxidation of alkenes is insignificant compared to typical daytime production rates of 0.3–0.5 ppb/h. Downwind of Mexico City, the possible nighttime production of  $\text{NO}_3$  and  $\text{N}_2\text{O}_5$  from observed  $\text{NO}_2$  and  $\text{O}_3$  is only a few ppt.

In summary, measured ratios of  $\Sigma\text{ANs}$  to  $\text{O}_x$  in Mexico City are high, corresponding to an average implied branching ratio of 7–10%, and are much larger than calculated based on observed and estimated hydrocarbons. We identify three poorly known possible candidates for reducing the modeled-measured difference: (a) the presence of unmeasured, long-chain compounds with high yields, (b) underestimates of nitrate yields from organic molecules and (c) higher rates of dinitrate formation than have previously been considered in other locations and show that all of them are consistent with the data. All three should be subject to further investigation.

#### 4.2 Evolution of the $\text{O}_x$ vs. $\Sigma\text{ANs}$ correlation

The calculated and observed  $\text{O}_x$  v.  $\Sigma\text{ANs}$  can generally only be directly compared in the near-field of a source region where production outweighs all other factors. As the plume ages the most reactive primary VOC are depleted, enhancing secondary OVOC and resulting in a mixture that produces ozone and  $\Sigma\text{ANs}$  in different ratios than the initial mixture does. These effects have been described previously for observations in Houston and Granite Bay where an increase in the slope of  $\text{O}_x/\Sigma\text{ANs}$  (a decrease in  $\alpha$ ) over the course of the day was interpreted as due to the increase in non-nitrate producing ozone precursors. The slope was higher in the afternoon because of increased concentrations of  $\text{O}_3$  precursors such as CO and  $\text{CH}_2\text{O}$  that are generated from the oxidation of other hydrocarbons but do not form nitrates upon oxidation. Similar processes are likely driving the variation in the slope of  $\Sigma\text{ANs}$  vs.  $\text{O}_x$  in the Mexico City plume as it evolves downwind. We do find that, although loss becomes more important over time, production outweighs loss for both  $\text{O}_x$  and  $\Sigma\text{ANs}$  over the entire range of photochemical ages sampled by the DC-8. As noted above, for  $\Sigma\text{ANs}$  the loss rate is  $\sim 2\%$ ,  $\sim 2.5\%$  and  $\sim 10\%$  of the instantaneous production rate at 0, 500 and 1000 km respectively. The instantaneous photochemical loss rate for  $\text{O}_x$  is never more than 0.5% of the production rate anywhere in the plume. In what follows

we use the observed evolution of the  $\Sigma\text{ANs}$  vs.  $\text{O}_x$  correlation and the  $\Sigma(\text{C}_1\text{--C}_5 \text{ nitrates})/\Sigma\text{ANs}$  ratio in conjunction with the calculated instantaneous production rates to assess the spatial extent to which the plume is impacted by the unknown chemistry identified in Sect. 4.1.

In order to compare the calculated instantaneous production rates to the observed  $\Sigma(\text{C}_1\text{--C}_5 \text{ nitrates})/\Sigma\text{ANs}$  ratio and  $\Sigma\text{ANs}$  vs.  $\text{O}_x$  correlation we must use a kind of stepwise integration. The instantaneous and observed slopes or ratios would only be expected to match exactly in the near-field of the source region over which the VOC mixture is invariant. As the plume ages and the VOC mixture changes, the observations reflect a linear combination of all of the previous instantaneous production rather than the single instantaneous slope calculated for a given point. For instance, in the case of the slope of the  $\Sigma\text{ANs}$  vs.  $\text{O}_x$  correlation, the observed slope after some number,  $n$ , of elapsed time intervals ( $\Delta t$ ) is given by:

$$M_n = \frac{\sum_{i=1}^n \Delta(\text{O}_x)_i \cdot \Delta t_i}{\sum_{i=1}^n \Delta(\Sigma\text{ANs})_i \cdot \Delta t_i}$$

Clearly for the first time interval, given correct chemistry, the overall slope ( $M_1$ ) should be similar to the instantaneous slope ( $\Delta(\text{O}_x)_1/\Delta(\Sigma\text{ANs})_1$ ). If the calculated and the observed slopes matched reasonably well for the first time interval we could simply calculate  $M_2$  using the equation above and compare it to the observed  $M_2$ . Since, however, the observed and calculated slopes are entirely dissimilar at point 1, the observed and calculated slopes at point 2 would be different regardless of whether the calculated instantaneous production was correct over  $\Delta t_2$  because the second step in the calculation is impacted by the error in the first. What we really want to assess is whether the calculated instantaneous production rates during  $\Delta t_2$  can explain the change between  $M_{1\text{obs}}$  and  $M_{2\text{obs}}$ . To do this we calculate  $M_n$  for  $n > 1$  using the observed  $M_{n-1}$  slope as follows:

$$M_{n\text{-calc}} \approx \frac{\left( M_{n-1\text{-obs}} \times \sum_{i=1}^{n-1} \Delta(\Sigma\text{ANs})_i + \Delta(\text{O}_x)_n \right)}{\left( \sum_{i=1}^n \Delta(\Sigma\text{ANs})_i \right)}$$

Figure 7a shows the observed  $\text{O}_x$  v.  $\Sigma\text{ANs}$  slope as compared to that expected based on stepwise integration of the calculated instantaneous  $\Sigma\text{ANs}$  and  $\text{O}_x$  production rates performed as described above. The first point shown in Fig. 7a is a direct comparison of the calculated instantaneous  $\text{O}_x/\Sigma\text{ANs}$  with the observed  $\text{O}_x/\Sigma\text{ANs}$  correlation in Mexico City. We then calculate successive slopes by combining the observed slope at the earlier time with the instantaneous production rate at the later time. This prevents an error in the initial condition from propagating through the entire calculation. The calculated slope in Mexico City and just downwind

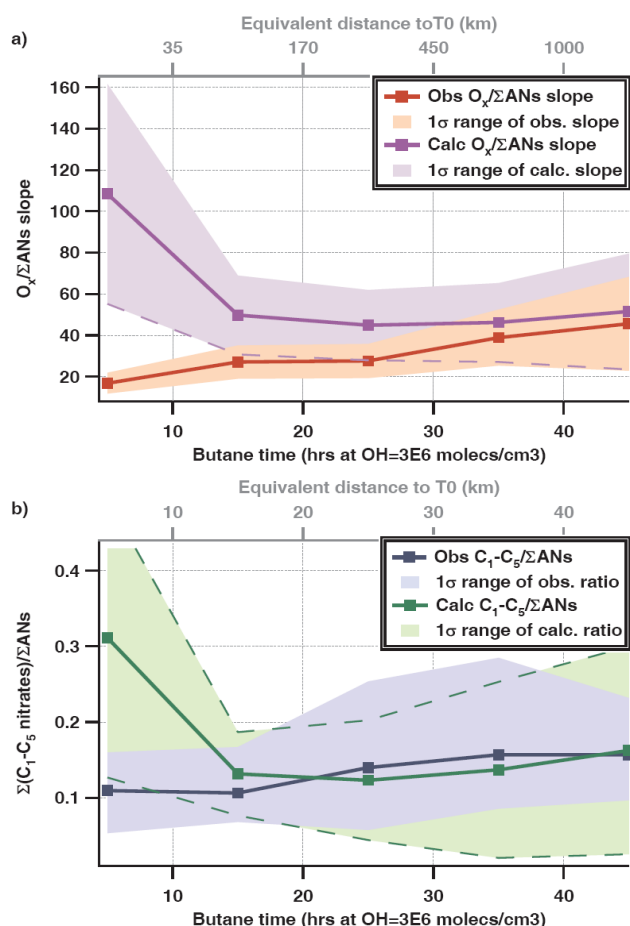


**Fig. 7.** (a) The observed (red) and calculated (purple)  $\Sigma\text{ANs}$  v.  $\text{O}_x$  slope as a function of photochemical age. Shaded areas represent the  $1\sigma$  variation of the data. (b) The observed (blue) and calculated (green)  $\Sigma(\text{C}_1\text{--C}_5 \text{ nitrates})/\Sigma\text{ANs}$  ratio as a function of photochemical age. Shaded areas, again, represent the  $1\sigma$  variation of the data.

is considerably higher than the observed slope but the agreement improves substantially by  $>30$  h of photochemical aging. Again, we can corroborate this result using the ratio of  $\Sigma(\text{C}_1\text{--C}_5 \text{ nitrates})/\Sigma\text{ANs}$  (Fig. 7b). The observed and calculated  $\Sigma(\text{C}_1\text{--C}_5 \text{ nitrates})/\Sigma\text{ANs}$  ratios converge within 15 h. Thus, the compounds responsible for the excess  $\Sigma\text{ANs}$  observed in Mexico City likely have short oxidative lifetimes and are consumed early in the plume evolution. Any of the above hypotheses would be consistent with this behavior.

### 4.3 Impacts of $\Sigma\text{ANs}$ chemistry on predicted $\text{O}_3$ production

The slope of  $\text{O}_x/\Sigma\text{ANs}$  was observed to be remarkably high in Mexico City as compared to other urban locations. The formation of alkyl and multifunctional nitrates affects our ability to predict  $\text{O}_3$  production both because it represents a direct alternative to the generation of  $\text{NO}_2$  and thus  $\text{O}_3$  from

the  $\text{RO}_2+\text{NO}$  reaction and because of the less direct feedback on  $\text{RO}_2$  and  $\text{HO}_2$  concentrations.  $\Sigma\text{ANs}$  formation has not been evaluated in detail in the current generation of chemical models, a fact we suggest should be remedied in the near future. Any regional or global model, aimed at predicting  $\text{O}_3$  concentrations, that fails to take this chemistry into account will over-predict  $\text{O}_3$  production as a result. We can estimate the magnitude of this effect using observed radical species and a series of simple equations. The instantaneous gross  $\text{O}_3$  production is defined as:

$$P(\text{O}_3) = [\text{NO}] \cdot (k_{\text{NO}+\text{HO}_2} \cdot [\text{HO}_2] + k_{\text{NO}+\text{RO}_2} \cdot [\text{RO}_2]) \quad (8)$$

We have measurements of  $\text{NO}$  and  $\text{HO}_2$  and we can calculate  $\text{RO}_2$  by assuming conservation of radicals and setting  $P(\text{HO}_x) = L(\text{HO}_x)$  where  $\text{HO}_x$  is defined as  $\text{OH}+\text{HO}_2+\text{RO}_2$ .  $\text{HO}_x$  production arises from the photolysis of  $\text{O}_3$  in the presence of water,  $\text{CH}_2\text{O}$  and  $\text{H}_2\text{O}_2$  with minor contributions from a number of oxygenated VOC's (OVOCs). For the analysis described here we have included photolysis of acetaldehyde, acetone, propanal, methanoic acid and  $\text{HNO}_3$  to give an overall  $\text{HO}_x$  production rate of:

$$P(\text{HO}_x) = 2J_{\text{O}_3 \rightarrow \text{O}_2 + \text{O}(^1\text{D})} [\text{O}_3] \frac{[\text{H}_2\text{O}]}{[M]} \quad (9)$$

$$+ 2J_{\text{CH}_2\text{O} \rightarrow \text{H} + \text{HCO}} [\text{CH}_2\text{O}] + 2J_{\text{H}_2\text{O}_2} [\text{H}_2\text{O}_2]$$

$$+ 2J_{\text{Acetaldehyde}} [\text{CH}_3\text{CHO}] + 2J_{\text{Acetone}} [\text{CH}_3\text{C}(\text{O})\text{CH}_3]$$

$$+ 2J_{\text{Pr opanal}} [\text{C}_2\text{H}_5\text{CHO}] + 2J_{\text{CH}_3\text{COOH}} [\text{CH}_3\text{COOH}]$$

$$+ J_{\text{HNO}_3} [\text{HNO}_3]$$

$\text{HO}_x$  loss occurs through production of  $\text{HNO}_3$ ,  $\Sigma\text{ANs}$  and organic peroxides ( $\text{HOOH}$ ,  $\text{ROOH}$  or  $\text{ROOR}$ ). The initiation reaction of  $\text{OH}+\text{RH}$  is not considered a  $\text{HO}_x$  loss because, although it consumes one molecule of  $\text{OH}$ , it results in the almost instantaneous production of an  $\text{RO}_2$  molecule. Production of  $\text{HNO}_3$  or an alkyl nitrate consumes a single  $\text{HO}_x$  molecule while production of hydrogen peroxide or organic peroxides consumes two  $\text{HO}_x$  molecules so  $L(\text{HO}_x)$  can be written as:

$$L(\text{HO}_x) = 2 \left( k_{\text{HO}_2+\text{HO}_2} [\text{HO}_2]^2 + k_{\text{RO}_2+\text{RO}_2} [\text{RO}_2]^2 \right) \quad (10)$$

$$+ k_{\text{HO}_2+\text{RO}_2} [\text{HO}_2][\text{RO}_2] + k_{\text{OH}+\text{NO}_2} [\text{OH}][\text{NO}_2]$$

$$+ \alpha k_{\text{RO}_2+\text{NO}} [\text{RO}_2][\text{NO}]$$

Where  $\alpha$  is the nitrate branching ratio. Setting  $P(\text{HO}_x) = L(\text{HO}_x)$  and inserting measured values of  $\text{OH}$ ,  $\text{HO}_2$ ,  $\text{NO}$  and  $\text{NO}_2$ , we can solve the quadratic equation to find the  $\text{RO}_2$  concentration. In what follows we have calculated  $\text{RO}_2$  for each of the times for which we extracted an effective branching ratio from the observations in Sect. 3.3 above. Taking a water concentration of 0.6%, we use  $k_{\text{OH}+\text{NO}_2} = 1.22 \times 10^{-11} \text{ cm}^3/\text{molec/s}$ ,  $k_{\text{HO}_2+\text{HO}_2} = 2.74 \times 10^{-12} \text{ cm}^3/\text{molec/s}$ ,  $k_{\text{HO}_2+\text{RO}_2} = 8 \times 10^{-12} \text{ cm}^3/\text{molec/s}$  and  $k_{\text{RO}_2+\text{RO}_2} = 6.8 \times 10^{-14} \text{ cm}^3/\text{molec/s}$  based on JPL evaluation number 15 (Sander

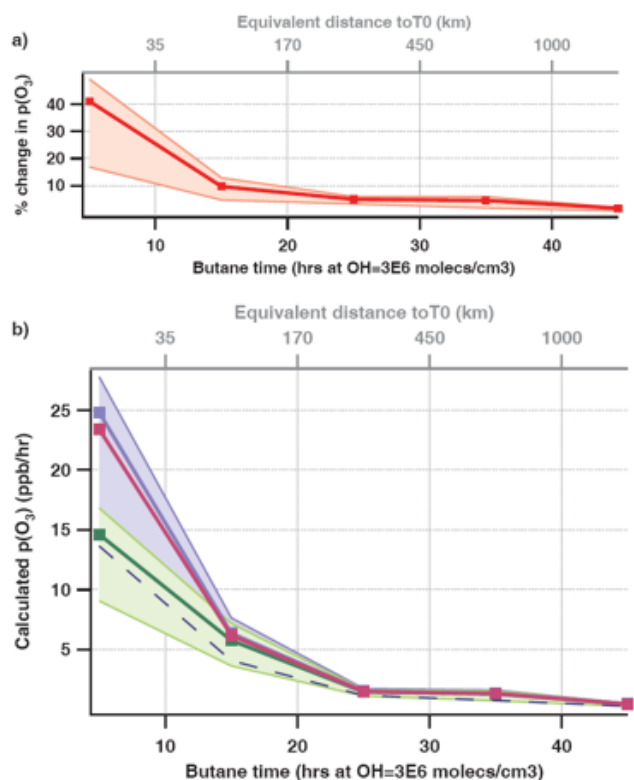


**Fig. 8.** (a) The median percent decrease in the calculated  $P(\text{O}_3)$  as a result of including  $\Sigma\text{ANs}$  formation with the observed average nitrate branching ratios. The borders of the shaded region represent the  $1\sigma$  variation of the data. (b) The absolute ozone production rate calculated using Eqs. (7) and (8) with no nitrate formation (blue), with nitrate formation using the branching ratio calculated using the MCM mechanism as shown in Table 1 (magenta) and with nitrate formation using the branching ratios inferred from observed slopes of  $\Sigma\text{ANs}$  vs.  $\text{O}_x$  in the Mexico City plume (green). Again, the shaded area represents the spread of the data from the  $1\sigma$  variation of the data.

et al., 2006) assuming generic  $\text{RO}_2$  behaves as  $\text{C}_2\text{H}_5\text{O}_2$ . It should be noted that the calculated  $\text{RO}_2$  concentration and therefore the calculated  $P(\text{O}_3)$  is sensitive to the assumed value of  $k_{\text{RO}_2+\text{RO}_2}$ . When  $\text{OH}+\text{NO}_2$  slow sufficiently to permit accumulation of peroxy radicals,  $\text{RO}_2$  is approximately equal to  $\text{HO}_2$  and  $\text{HO}_2+\text{RO}_2$  is the most important of the three peroxide formation reactions. We use the median observed values of  $\text{OH}$ ,  $\text{HO}_2$ ,  $\text{NO}$  and  $\text{NO}_2$  and calculate  $\text{RO}_2$  concentrations using both the inferred  $\alpha$ 's and  $\alpha=0$ . We then use these  $\text{RO}_2$  concentrations to calculate  $P(\text{O}_3)$ .

The top panel of Fig. 8 shows the percent change in calculated  $P(\text{O}_3)$  as a result of including the formation of  $\Sigma\text{ANs}$ . Near Mexico City, where alkyl nitrate production is high, the effect of including this chemistry in a model is to reduce the calculated  $P(\text{O}_3)$  by 40%. The bottom panel of Fig. 8 shows  $P(\text{O}_3)$  using  $\alpha=0$  (blue squares and line), using  $\alpha$ 's as would be calculated using the MCM and observed hydrocar-

bons (magenta squares and line) and using the  $\alpha$ 's inferred from the  $\text{O}_x/\Sigma\text{ANs}$  correlation (green squares and line). The effect persists, albeit minorly, downwind of the city and the integrated effect of neglecting alkyl nitrate formation leads to significant errors in the calculated  $\text{O}_3$  production over the lifetime of the megacity plume.

## 5 Conclusions

$\Sigma\text{ANs}$  have been observed to be a significant ( $\sim 10\%$ ) fraction of  $\text{NO}_y$  in the immediate vicinity and well downwind of Mexico City. Hundreds of ppts of  $\Sigma\text{ANs}$  were observed over the Gulf of Mexico. The  $\Sigma\text{ANs}$  fraction of  $\text{NO}_y$  increases with increasing photochemical age and indicates continued production of  $\Sigma\text{ANs}$  far from the source region. The source of  $\Sigma\text{ANs}$  is larger in the Mexico City plume than in other urban locations. The effect of  $\Sigma\text{ANs}$  on calculated  $P(\text{O}_3)$  is  $\sim 30\%$ , a value that is unexpectedly large and that implies careful consideration should be given to the role of  $\Sigma\text{AN}$  formation in discussion of any  $\text{O}_3$  control strategies. We find that these observations of high  $\Sigma\text{AN}$  concentrations require one of more of the following: the presence of unmeasured, long-chain hydrocarbons with high nitrate formation rates, underestimates in nitrate formation rates for some fraction of the measured compounds, and/or a larger role for the formation of di-nitrates than has been considered previously. The evolution of the plume downwind indicates that the unknown compounds responsible are relatively short-lived.

*Acknowledgements.* The work presented here was funded by NASA headquarters under the NASA Earth Systems Science Fellowship Program and by NASA grant #NAG5-13668. The authors would also like to sincerely thank Brian Heikes and Alan Fried for the use of their formaldehyde data, Melody Avery for the use of her ozone data, Bill Brune for the use of his  $\text{HO}_x$  measurements and Greg Huey for the use of his  $\text{NO}$  measurements.

Edited by: A. Hofzumahaus

## References

- Altchuller, A. P.: PANs in the Atmosphere, *J. Air Waste Manage. Assoc.*, 43, 1221–1230, 1993.
- Bertman, S. B., Roberts, J. M., Parrish, D. D., Buhr, M. P., Goldan, P. D., Kuster, W. C., Fehsenfeld, F. C., Montzka, S. A., and Westberg, H.: Evolution Of Alkyl Nitrates With Air-Mass Age, *J. Geophys. Res.-Atmos.*, 100(D11), 22805–22813, 1995.
- Bertram, T. H., Cohen, R. C., Thorn, W. J., and Chu, P. M.: Consistency of ozone and nitrogen oxides standards at tropospherically relevant mixing ratios, *J. Air Waste Manage. Assoc.*, 55, 1473–1479, 2005.
- Bloss, C., Wagner, V., Jenkin, M. E., Volkamer, R., Bloss, W. J., Lee, J. D., Heard, D. E., Wirtz, K., Martin-Reviejo, M., Rea, G., Wenger, J. C., and Pilling, M. J.: Development of a detailed chemical mechanism (MCMv3.1) for the atmospheric oxidation

- of aromatic hydrocarbons, *Atmos. Chem. Phys.*, 5, 641–664, doi:10.5194/acp-5-641-2005, 2005.
- Carter, W. P. L. and Atkinson, R.: Alkyl nitrate formation from the atmospheric photooxidation of alkanes – a revised estimation method, *J. Atmos. Chem.*, 8, 165–173, 1989.
- Cleary, P. A., Wooldridge, P. J., and Cohen, R. C.: Laser-induced fluorescence detection of atmospheric  $\text{NO}_2$  with a commercial diode laser and a supersonic expansion, *Appl. Optics*, 41, 6950–6956, 2002.
- Cleary, P. A., Murphy, J. G., Wooldridge, P. J., Day, D. A., Millet, D. B., McKay, M., Goldstein, A. H., and Cohen, R. C.: Observations of total alkyl nitrates within the Sacramento Urban Plume, *Atmos. Chem. Phys. Discuss.*, 5, 4801–4843, doi:10.5194/acpd-5-4801-2005, 2005.
- Colman, J. J., Swanson, A. L., Meinardi, S., Sive, B. C., Blake, D. R., and Rowland, F. S.: Description of the analysis of a wide range of volatile organic compounds in whole air samples collected during PEM-Tropics A and B, *Anal. Chem.*, 73, 3723–3731, 2001.
- Day, D. A., Wooldridge, P. J., Dillon, M. B., Thornton, J. A., and Cohen, R. C.: A thermal dissociation laser-induced fluorescence instrument for in situ detection of  $\text{NO}_2$ , peroxy nitrates, alkyl nitrates and  $\text{HNO}_3$ , *J. Geophys. Res.-Atmos.*, 107, 4046, doi:10.1029/2001JD000779, 2002.
- Day, D. A., Dillon, M. B., Wooldridge, P. J., Thornton, J. A., Rosen, R. S., Wood, E. C., and Cohen, R. C.: On alkyl nitrates,  $\text{O}_3$ , and the “missing  $\text{NO}_y$ ”, *J. Geophys. Res.-Atmos.*, 108, ACH7-1-10, doi:10.1029/2003JD003685, 2003.
- Dibb, J. E., Scheuer, E., Avery, M., Plant, J., and Sachse, G.: In situ evidence for renitrification in the Arctic lower stratosphere during the polar aura validation experiment (PAVE), *Geophys. Res. Lett.*, 33, L12815, doi:10.1029/2006GL026243, 2006.
- Dunlea, E. J., Herndon, S. C., Nelson, D. D., Volkamer, R. M., San Martini, F., Sheehy, P. M., Zahniser, M. S., Shorter, J. H., Wormhoudt, J. C., Lamb, B. K., Allwine, E. J., Gaffney, J. S., Marley, N. A., Grutter, M., Marquez, C., Blanco, S., Cardenas, B., Retama, A., Ramos Villegas, C. R., Kolb, C. E., Molina, L. T., and Molina, M. J.: Evaluation of nitrogen dioxide chemiluminescence monitors in a polluted urban environment, *Atmos. Chem. Phys.*, 7, 2691–2704, doi:10.5194/acp-7-2691-2007, 2007.
- Dusanter, S., Vimal, D., Stevens, P. S., Volkamer, R., and Molina, L. T.: Measurements of OH and  $\text{HO}_2$  concentrations during the MCMA-2006 field campaign - Part 1: Deployment of the Indiana University laser-induced fluorescence instrument, *Atmos. Chem. Phys.*, 9, 1665–1685, doi:10.5194/acp-9-1665-2009, 2009.
- Faloona, I. C., Tan, D., Leshner, R. L., Hazen, N. L., Frame, C. L., Simpas, J. B., Harder, H., Martinez, M., Di Carlo, P., Ren, X. R., and Brune, W. H.: A laser-induced fluorescence instrument for detecting tropospheric OH and  $\text{HO}_2$ : Characteristics and calibration, *J. Atmos. Chem.*, 47, 139–167, 2004.
- Farmer, D. K. and Cohen, R. C.: Observations of  $\text{HNO}_3$ ,  $\Sigma\text{AN}$ ,  $\Sigma\text{PN}$  and  $\text{NO}_2$  fluxes: evidence for rapid  $\text{HO}_x$  chemistry within a pine forest canopy, *Atmos. Chem. Phys.*, 8, 3899–3917, doi:10.5194/acp-8-3899-2008, 2008.
- Fountoukis, C., Nenes, A., Sullivan, A., Weber, R., Van Reken, T., Fischer, M., Matas, E., Moya, M., Farmer, D., and Cohen, R. C.: Thermodynamic characterization of Mexico City aerosol during MILAGRO 2006, *Atmos. Chem. Phys.*, 9, 2141–2156, doi:10.5194/acp-9-2141-2009, 2009.
- Fried, A., Wang, Y. H., Cantrell, C., Wert, B., Walega, J., Ridley, B., Atlas, E., Shetter, R., Lefer, B., Coffey, M. T., Hannigan, J., Blake, D., Blake, N., Meinardi, S., Talbot, B., Dibb, J., Scheuer, E., Wingenter, O., Snow, J., Heikes, B., and Ehhalt, D.: Tunable diode laser measurements of formaldehyde during the TOPSE 2000 study: Distributions, trends and a model comparison, *J. Geophys. Res.-Atmos.*, 108, 8365, doi:10.1029/2002JD002208, 2003.
- Fuchs, H., Ball, S. M., Bohn, B., Brauers, T., Cohen, R. C., Dorn, H.-P., Dubé, W. P., Fry, J. L., Häsel, R., Heitmann, U., Jones, R. L., Kleffmann, J., Mentel, T. F., Müsgen, P., Rohrer, F., Rollins, A. W., Ruth, A. A., Kiendler-Scharr, A., Schlosser, E., Shillings, A. J. L., Tillmann, R., Varma, R. M., Venables, D. S., Villena Tapia, G., Wahner, A., Wegener, R., Wooldridge, P. J., and Brown, S. S.: Intercomparison of measurements of  $\text{NO}_2$  concentrations in the atmosphere simulation chamber SAPHIR during the  $\text{NO}_3\text{Comp}$  campaign, *Atmos. Meas. Tech.*, 3, 21–37, doi:10.5194/amt-3-21-2010, 2010.
- Fuelberg, H. E., Porter, M. J., Kiley, C. M., Halland, J. J., and Morse, D.: Meteorological conditions and anomalies during the Intercontinental Chemical Transport Experiment-North America, *J. Geophys. Res.-Atmos.*, 112, D12S06, doi:10.1029/2006JD007734, 2007.
- Giacopelli, P., Ford, K., Espada, C., and Shepson, P. B.: Comparison of the measured and simulated isoprene nitrate distributions above a forest canopy, *J. Geophys. Res.-Atmos.*, 110, D01304, doi:10.1029/2004JD005123, 2005.
- Hamilton, J. F., Lewis, A. C., Bloss, C., Wagner, V., Henderson, A. P., Golding, B. T., Wirtz, K., Martin-Reviejo, M., and Pilling, M. J.: Measurements of photo-oxidation products from the reaction of a series of alkyl-benzenes with hydroxyl radicals during EXACT using comprehensive gas chromatography, *Atmos. Chem. Phys.*, 3, 1999–2014, doi:10.5194/acp-3-1999-2003, 2003.
- Heikes, B. G.: Formaldehyde And Hydroperoxides At Mauna-Loa Observatory, *J. Geophys. Res.-Atmos.*, 97(D16), 18001–18013, 1992.
- Horowitz, L. W., Fiore, A. M., Milly, G. P., Cohen, R. C., Perring, A., Wooldridge, P. J., Hess, P. G., Emmons, L. K., and Lamarque, J. F.: Observational constraints on the chemistry of isoprene nitrates over the eastern United States, *J. Geophys. Res.-Atmos.*, 112, D12S08, doi:10.1029/2006JD007747, 2007.
- Ito, A., Sillman, S., and Penner, J. E.: Effects of additional non-methane volatile organic compounds, organic nitrates, and direct emissions of oxygenated organic species on global tropospheric chemistry, *J. Geophys. Res.-Atmos.*, 112, D06309, doi:10.1029/2005JD006556, 2007.
- Jenkin, M. E., Saunders, S. M., Wagner, V., and Pilling, M. J.: Protocol for the development of the Master Chemical Mechanism, MCM v3 (Part B): tropospheric degradation of aromatic volatile organic compounds, *Atmos. Chem. Phys.*, 3, 181–193, doi:10.5194/acp-3-181-2003, 2003.
- LaFranchi, B. W., Wolfe, G. M., Thornton, J. A., Harrold, S. A., Browne, E. C., Min, K. E., Wooldridge, P. J., Gilman, J. B., Kuster, W. C., Goldan, P. D., de Gouw, J. A., McKay, M., Goldstein, A. H., Ren, X., Mao, J., and Cohen, R. C.: Closing the peroxy acetyl nitrate budget: observations of acyl peroxy nitrates (PAN, PPN, and MPAN) during BEARPEX 2007, *Atmos. Chem. Phys.*, 9, 7623–7641, doi:10.5194/acp-9-7623-2009, 2009.
- Molina, L. T., Madronich, S., Gaffney, J. S., Apel, E., de Foy,

- B., Fast, J., Ferrare, R., Herndon, S., Jimenez, J. L., Lamb, B., Osornio-Vargas, A. R., Russell, P., Schauer, J. J., Stevens, P. S., and Zavala, M.: An overview of the MILAGRO 2006 campaign: Mexico City emissions and their transport and transformation, *Atmos. Chem. Phys. Discuss.*, 10, 7819–7983, doi:10.5194/acpd-10-7819-2010, 2010.
- Murphy, J. G., Day, D. A., Cleary, P. A., Wooldridge, P. J., and Cohen, R. C.: Observations of the diurnal and seasonal trends in nitrogen oxides in the western Sierra Nevada, *Atmos. Chem. Phys.*, 6, 5321–5338, doi:10.5194/acp-6-5321-2006, 2006.
- Paulot, F., Crouse, J. D., Kjaergaard, H. G., Kroll, J. H., Seinfeld, J. H., and Wennberg, P. O.: Isoprene photooxidation: new insights into the production of acids and organic nitrates, *Atmos. Chem. Phys.*, 9, 1479–1501, doi:10.5194/acp-9-1479-2009, 2009.
- Parrish, D. D., Kuster, W. C., Shao, M., Yokouchi, Y., Kondo, Y., Goldan, P. D., de Gouw, J. A., Koike, M., and Shirai, T.: Comparison of air pollutant emissions among mega-cities, *Atmos. Environ.*, 43(40), 6435–6441, 2009.
- Perring, A. E., Bertram, T. H., Wooldridge, P. J., Fried, A., Heikes, B. G., Dibb, J., Crouse, J. D., Wennberg, P. O., Blake, N. J., Blake, D. R., Brune, W. H., Singh, H. B., and Cohen, R. C.: Airborne observations of total  $\text{RONO}_2$ : new constraints on the yield and lifetime of isoprene nitrates, *Atmos. Chem. Phys.*, 9, 1451–1463, doi:10.5194/acp-9-1451-2009, 2009a.
- Perring, A. E., Wisthaler, A., Graus, M., Wooldridge, P. J., Lockwood, A. L., Mielke, L. H., Shepson, P. B., Hansel, A., and Cohen, R. C.: A product study of the isoprene +  $\text{NO}_3$  reaction, *Atmos. Chem. Phys.*, 9, 4945–4956, doi:10.5194/acp-9-4945-2009, 2009b.
- Robinson, A. L., Donahue, N. M., Shrivastava, M. K., Weitkamp, E. A., Sage, A. M., Grieshop, A. P., Lane, T. E., Pierce, J. R., and Pandis, S. N.: Rethinking organic aerosols: Semivolatile emissions and photochemical aging, *Science*, 315, 1259–1262, 2007.
- Rosen, R. S., Wood, E. C., Wooldridge, P. J., Thornton, J. A., Day, D. A., Kuster, W., Williams, E. J., Jobson, B. T., and Cohen, R. C.: Observations of total alkyl nitrates during Texas Air Quality Study 2000: Implications for  $\text{O}_3$  and alkyl nitrate photochemistry, *J. Geophys. Res.-Atmos.*, 109, D07303, doi:10.1029/2003JD004227, 2004.
- Sachse, G. W., Hill, G. F., Wade, L. O., and Perry, M. G.: Fast-response, High-precision carbon-monoxide sensor using a tunable diode-laser absorption technique, *J. Geophys. Res.-Atmos.*, 92(D2) 2071–2081, 1987.
- Sander, S. P., Finlayson-Pitts, B. J., Friedl, R. R., Golden, D. M., Huie, R. E., Keller-Rudek, H., Kolb, C. E., Kurylo, M. J., Molina, M. J., Moortgat, G. K., Orkin, V. L., Ravishankara, A. R. and Wine, P. H.: “Chemical Kinetics and Photochemical Data for Use in Atmospheric Studies, Evaluation Number 15”, JPL Publication 06-2, Jet Propulsion Laboratory, Pasadena, 2006.
- Scheuer, E. M., Talbot, R. W., Dibb, J., Seid, G. K., Debell, L., and Lefer, B.: Seasonal distributions of fine aerosol sulfate in the North American Arctic basin during TOPSE, *J. Geophys. Res.-Atmos.*, 108(D4), 8370, doi:10.1029/2001JD001364, 2003.
- Shetter, R. E. and Muller, M.: Photolysis frequency measurements using actinic flux spectroradiometry during the PEM-Tropics mission: Instrumentation description and some results, *J. Geophys. Res.-Atmos.*, 104(D5), 5647–5661, 1999.
- Singh, H. B. and Salas, L. J.: Measurements Of Peroxyacetyl Nitrate (Pan) And Peroxypropionyl Nitrate (PPN) At Selected Urban, Rural And Remote Sites, *Atmos. Environ.*, 23, 231–238, 1989.
- Singh, H. B., Thompson, A. M., and Schlager, H.: SONEX airborne mission and coordinated POLINAT-2 activity: overview and accomplishments, *Geophys. Res. Lett.*, 26, 3053–3056, 1999.
- Singh, H. B., Brune, W. H., Crawford, J. H., Flocke, F., and Jacob, D. J.: Chemistry and transport of pollution over the Gulf of Mexico and the Pacific: spring 2006 INTEX-B campaign overview and first results, *Atmos. Chem. Phys.*, 9, 2301–2318, doi:10.5194/acp-9-2301-2009, 2009.
- Talbot, R., Dibb, J., Scheuer, E., Seid, G., Russo, R., Sandholm, S., Tan, D., Singh, H., Blake, D., Blake, N., Atlas, E., Sachse, G., Jordan, C., and Avery, M.: Reactive nitrogen in Asian continental outflow over the western Pacific: Results from the NASA Transport and Chemical Evolution over the Pacific (TRACE-P) airborne mission, *J. Geophys. Res.-Atmos.*, 108, GTE24-1-17, doi:10.1029/2002JD003129, 2003.
- Thornton, J. A., Wooldridge, P. J., and Cohen, R. C.: Atmospheric  $\text{NO}_2$ : In situ laser-induced fluorescence detection at parts per trillion mixing ratios, *Anal. Chem.*, 72, 528–539, 2000.
- Thornton, J. A., Wooldridge, P. J., Cohen, R. C., Williams, E. J., Hereid, D., Fehsenfeld, F. C., Stutz, J., and Alicke, B.: Comparisons of in situ and long path measurements of  $\text{NO}_2$  in urban plumes, *J. Geophys. Res.-Atmos.*, 108, 4496, doi:10.1029/2003JD003559, 2003.
- Wagner, V., Jenkin, M. E., Saunders, S. M., Stanton, J., Wirtz, K., and Pilling, M. J.: Modelling of the photooxidation of toluene: conceptual ideas for validating detailed mechanisms, *Atmos. Chem. Phys.*, 3, 89–106, doi:10.5194/acp-3-89-2003, 2003.
- Warneke, C., de Gouw, J. A., Goldan, P. D., Kuster, W. C., Williams, E. J., Lerner, B. M., Jakoubek, R., Brown, S. S., Stark, H., Aldener, M., Ravishankara, A. R., Roberts, J. M., Marchewka, M., Bertmen, S., Sueper, D. T., McKeen, S. A., Meagher, J. F., and Fehsenfeld, F. C.: Comparison of daytime and nighttime oxidation of biogenic and anthropogenic VOCs along the New England coast in summer during New England Air Quality Study 2002, *J. Geophys. Res.-Atmos.*, 109, D10309, doi:10.1029/2003JD004424, 2004.
- Wooldridge, P. J., Perring, A. E., Bertram, T. H., Flocke, F. M., Roberts, J. M., Singh, H. B., Huey, L. G., Thornton, J. A., Wolfe, G. M., Murphy, J. G., Fry, J. L., Rollins, A. W., LaFranchi, B. W., and Cohen, R. C.: Total Peroxy Nitrates ( $\Sigma\text{PNs}$ ) in the atmosphere: the Thermal Dissociation-Laser Induced Fluorescence (TD-LIF) technique and comparisons to speciated PAN measurements, *Atmos. Meas. Tech.*, 3, 593–607, doi:10.5194/amt-3-593-2010, 2010.
- Wu, S. L., Mickle, L. J., Jacob, D. J., Logan, J. A., Yantosca, R. M., and Rind, D.: Why are there large differences between models in global budgets of tropospheric ozone?, *J. Geophys. Res.-Atmos.*, 112, D05302, doi:10.1029/2006JD007801, 2007.
- Wyche, K. P., Monks, P. S., Ellis, A. M., Cordell, R. L., Parker, A. E., Whyte, C., Metzger, A., Dommen, J., Duplissy, J., Prevot, A. S. H., Baltensperger, U., Rickard, A. R., and Wulfert, F.: Gas phase precursors to anthropogenic secondary organic aerosol: detailed observations of 1,3,5-trimethylbenzene photooxidation, *Atmos. Chem. Phys.*, 9, 635–665, doi:10.5194/acp-9-635-2009, 2009.